Structure and Cycle of Decadal Variability of Upper-Ocean Temperature in the North Pacific

RONG-HUA ZHANG AND SYDNEY LEVITUS

Ocean Climate Laboratory, National Oceanographic Data Center/NOAA, Silver Spring, Maryland

(Manuscript received 13 November 1995, in final form 9 September 1996)

ABSTRACT

Yearly upper-ocean in situ temperature anomaly data for the period 1961–90 are analyzed to reveal spatial structure and evolution of decadal variability in the North Pacific Ocean. An EOF analysis has been performed on individual temperature anomaly fields at upper-ocean standard levels, as well as simultaneously on the entire upper-ocean data to depict the combined three-dimensional structure in a coherent manner. Time evolution of anomaly fields is depicted by using a regression analysis.

The analyses detect the principal basin-scale structure of decadal warm period (DWP) and decadal cold period (DCP). There is a well-defined subsurface thermal anomaly pattern, characterized by a prominent seesaw structure with opposite anomaly polarity between the midlatitude North Pacific and the subtropical regions. During a DWP, a positive temperature anomaly is found in the central midlatitude upper ocean, with the maximum at about 100-m depth. This is accompanied by a corresponding negative anomaly in the American coastal region and in the subtropics. A reverse pattern of these anomalies is observed during the DCP. Evolution between the DWP and the DCP involves significant zonal and meridional propagation of anomaly phase around the North Pacific, showing consistent and coherent variations from subsurface to sea surface, from central midlatitudes to the American coastal regions, and to the subtropical Pacific Ocean. This phase propagation is much more well-organized at subsurface depths than that at the sea surface, suggesting an anomaly decadal-scale cycle circulating clockwise around the subtropical gyre, which supports earlier findings by Latif and Barnett. There is a systematic and coherent westward transpacific phase propagation in the subtropical region.

These analyses present evidence of the manner in which upper-ocean temperature anomalies evolved in the North Pacific, thus providing an observational basis for evaluating theoretical studies and model simulations. The dynamical implication for physical understanding and prediction of decadal climate variability are discussed.

1. Introduction

Understanding and interpreting natural climate variability is important not only for its intrinsic scientific merit, but also for assessing possibly forced climate variability such as global warming in response to an increase in greenhouse gases. Decadal variability in the ocean has recently received significant attention (IOC 1992). Extensive observational research has been conducted to describe its space–time evolution and to understand the physical processes and mechanisms that govern such oscillations in the North Atlantic Ocean (Bjerknes 1964; Dickson et al. 1988; Levitus 1989; Levitus 1990; Antonov 1993; Kushnir 1994; Levitus et al. 1994a, b, 1995).

Decadal climate variations in the North Pacific Ocean have long been of interest and are an active field for scientific research (Namias 1959; White and Barnett 1972; Haney 1980; Barnett 1981). Significant decadal-scale signals have been detected from observational data. One well-known example is the 1976–77 climate shift of the Pacific ocean–atmosphere system (Nitta and Yamada 1989; Ebbesmeyer et al. 1991; Miller et al. 1994a; Trenberth and Hurrel 1994). Sea surface temperatures (SSTs) exhibit decadal changes and have been analyzed in detail (Nitta and Yamada 1989; Cayan 1992; Tanimoto et al. 1993; Kawamura 1994; Wang 1995). Specifically, EOF analyses of SST data describe the spatial structure and time evolution of decadal-scale warm period (DWP) and cold period (DCP). The dominant modal pattern in the North Pacific Ocean shows an elliptical shape located in the central midlatitudes, accompanied by an opposite polarity around it. The time variations clearly show termination of a multiyear warm state during 1976–77 over the central midlatitudes with a sharp transition to a cold state, which persists for about a decade. This cooling in the central midlatitudes is accompanied by warming off the west coast of North America. Recently, analyses of subsurface ocean thermal data have documented changes in subsurface thermal structure (Watanabe and Mizuno 1992). In particular, Levitus et al. (1994b) describe the spatial patterns

Corresponding author address: Dr. Rong-Hua Zhang, Graduate School of Oceanography, University of Rhode Island, Narragansett, RI 02882.
E-mail: zrh@sequan.gso.uri.edu

of the most recurrent subsurface decadal thermal variability, characterized by an anomaly in the central midlatitude North Pacific, which is opposite in sign to anomaly in the region along the periphery of the subtropical gyre. Deser et al. (1996) present a detailed analysis of the vertical structure of seasonal thermal anomalies in the upper North Pacific Ocean during 1970–91, emphasizing the role of local interactions between the surface mixed layer and the thermocline in producing subsurface thermal anomalies. Zhang (1996, submitted to *Nature*) shows subsurface evidence of decadal climate variability in the North Pacific Ocean.

Although seasonal and interannual variations are well documented and understood, there is little understanding of decadal variability of three-dimensional upper-ocean thermal structure on basin scales. Its cause is not clear and the role of the subsurface ocean in decadal variability of the Pacific climate system is in debate. Numerous modeling studies in the last decade have been conducted to describe the structure and evolution and to elucidate the physical processes and mechanism responsible for the phenomenon (Yamagata and Masumoto 1992; Luksch and von Storch 1992; Graham 1994; von Storch 1994; Miller et al. 1994b; Jacobs et al. 1994; Latif and Barnett 1994, 1996). Although there are obvious discrepancies in comparison of simulated results with the corresponding observations, these studies have greatly improved our understanding of the observed phenomenon. At the same time, they also show a great sensitivity of model results to physical parameters, model formulation, and experiment design, giving rise to significant intermodel differences. For example, some studies suggest an atmosphere-driven mechanism for the mid- and high-latitude decadal variations through atmospheric teleconnection from the tropical Pacific Ocean (Bjerknes 1969; Trenberth and Hurrell 1994; Graham 1994; Miller et al. 1994b) but there is no answer to the fundamental question of how the decadal variations in the tropical Pacific originate. On the other hand, Latif and Barnett (1994, 1996) develop a consistent physical picture of how decadal climate variability over the Pacific can be generated, involving subsurface ocean dynamics and a coupled instability of the midlatitude ocean–atmosphere system. The cyclic evolution of thermal anomalies in the ocean is also evident in numerical simulations presented by von Storch (1994). Given the uncertainties of modeling and theoretical studies, it is necessary to analyze basin-wide subsurface thermal data in order to describe and understand decadal variability of upper-ocean thermal structure. Such data are becoming more abundant due to international efforts to increase the comprehensiveness of historical oceanographic databases (Levitus et al. 1994c).

The yearly temperature anomaly fields for the upper ocean produced by Levitus et al. (1994b) allow for a systematic description of large-scale, three-dimensional structure and evolution of temperature anomalies in the North Pacific. Such data analyses may improve our understanding of the role of subsurface ocean in decadal variability and shed light on some questions not yet answered. For example, what processes maintain persistent decadal-scale climate anomalies such as the DWP and DCP, and what mechanisms cause a relatively abrupt interdecadal change (phase transition) between them?

A brief description of the data sources and processing procedures is given in section 2. In section 3, some structure and evolution characteristics of decadal temperature variations are described. Using results of empirical orthogonal function (EOF) analyses, the dominant structure of the decadal temperature variability is further examined in section 4 through section 5. Its time evolution is investigated by a regression analysis in section 6. Finally, section 7 gives conclusions and discusses results.

2. Upper-ocean temperature data

The data used in the paper were the yearly in situ temperature anomaly fields described by Levitus et al. (1994b). These fields represented objective analyses of all historical temperature profiles available at the National Oceanographic Data Center (NODC/NOAA) through December 1993. These observational profiles have been analyzed in a consistent, objective manner on a 1° lat–long grid at standard oceanographic analysis levels between the sea surface and a depth of 400 m.

Briefly, the observed temperature profiles were subjected to quality control checks to identify any unrealistic data. After this, they were vertically interpolated to standard levels. The annual cycle is removed from the dataset by subtracting the climatological monthly mean 1° square temperature value at each standard level from the synoptic value of each profile. The anomaly profiles were then composited by 1-yr periods on a 1° grid at each upper-ocean standard level and for each year for the 1960–90. Finally, these 1° square anomaly fields were objectively analyzed with the same objective analysis scheme used by Levitus and Boyer (1994) to produce values on a regular 1° lat–long grid. Data sources, quality control, and analyses procedures were described in detail by Levitus and Boyer (1994) and by Boyer and Levitus (1994). One difference was that the first-guess field for each yearly anomaly analysis was defined to be zero for all 1° × 1° grid points. The distribution of temperature observations at selected upper-ocean standard levels each year from 1960 to 1990 were given by Levitus et al. (1994b).

For the present paper, we prepared datasets on a 5° lat–long grid by averaging the actual temperature anomalies from 1° lat–long grid values, giving no weight to a grid point without observations. The 5° grid points were centered at 2.5°N, 7.5°N, 12.5°N, . . . , in latitude, and at 122.5°E, 127.5°E, 132.5°E, . . . , in longitude. The analyses in the present paper are for the 1961–90 period. To produce yearly anomaly fields, 30-yr averaged values for 1961–90 were subtracted from those for

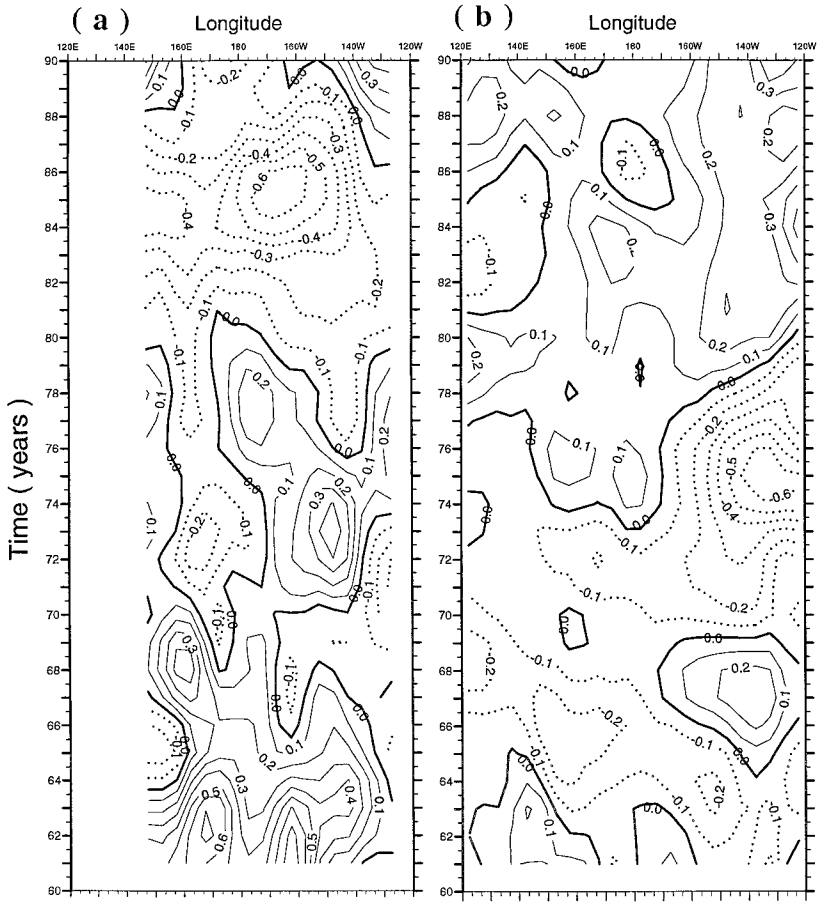

FIG. 1. Decadal variations in SST from 1961 to 1990 along (a) 42.5°N and along (b) 22.5°N, respectively. The contour interval is 0.1°C with a dotted line representing negative values.

each individual year. Then a 3-yr running mean of these yearly anomalies was performed before the analyses.

3. Decadal variation

Figure 1 shows the time variations in SST along 42.5°N and along 22.5°N. Decadal changes can be clearly seen. Along 22.5°N, the region east of 160°W exhibits a negative anomaly during the 1970s with a magnitude of −0.6°C. This region shifts to a positive anomaly by 1980. Along 42.5°N a positive anomaly occurs in the central Pacific during the 1970s and shifts to a negative anomaly by 1980.

Significant decadal variations are evident at subsurface ocean depths. With increasing depth, there are changes in both the structure and evolution features. The variability of temperature at subsurface depths is more organized and phase propagation characteristics are more evident as compared to the sea surface. Figure 2 exhibits the decadal fluctuations of temperature at 250-m depth along 42.5°N and along 22.5°N in longitudes, and along 162.5°E and 142.5°W in latitudes, respectively. Large decadal variations appear not only in the midlatitude North Pacific but also in the subtropics, with systematic and coherent phase differences between these two regions. The pattern of temperature variability tends to be well-organized at this depth with significant phase propagation and coherent variations on the basin scale. While the space–time evolution in the midlatitudes is largely dominated by a standing pattern, that in the subtropical Pacific has a discernible phase propagation, with structural differences in longitude from west to east. In particular, a westward trans-Pacific phase propagation can be detected along 22.5°N (Fig. 2b). In addition to the zonal phase propagation, meridional phase propagation occurs: northward in the subtropical western Pacific but southward in the east (Figs. 2c–d).

More detailed basinwide structure and evolution can be seen from the geographic distribution of temperature anomalies given by Levitus et al. (1994b). As an example, Fig. 3 shows horizontal distributions of temperature anomalies at 250-m depth in the North Pacific Ocean for year (a) 1970, (b) 1974, (c) 1978, (d) 1982, (e) 1986, and (f) 1990. The corresponding longitude–depth sections along 42.5°N and 22.5°N are given in Fig. 4. A striking feature is well-defined subsurface ther-

mal anomaly patterns and their orderly evolution with time. There are coherent phase differences in the anomalies between the central midlatitudes and the North American coast, and between the midlatitudes and the subtropics. These subsurface anomaly fields are sometime overlain by relatively shallow (0–50 m) anomaly fields of the opposite sign. Combining these figures together, the three-dimensional structure and evolution of upper-ocean temperature anomalies are evident. A clockwise rotation of the temperature anomalies can be visually detected at 250-m depth around the entire North Pacific: westward movement in the subtropics, northward in the west, eastward in the north, and southward in the east. During 1962–76, a decadal-scale warm period (DWP) prevails in the North Pacific Ocean: there is a positive anomaly in the western and central midlatitudes, and a negative anomaly in the subtropical western Pacific. The anomaly pattern reverses sign around 1976–77, that is, a transition takes place from DWP to DCP. The positive anomaly in the north appears to extend eastward and move southward in the eastern Pacific, while the negative anomaly in the south moves westward across the subtropics. Subsequently, the negative anomaly appears to continue its northward movement in the western boundary region and extends eastward along the Kuroshio Extension. Consequently, the warm conditions in the north decay and are replaced by a negative anomaly that persists thereafter for about a decade, with opposite anomaly polarity in the midlatitudes and subtropics. In the late 1980s, another transition occurs from DCP to DWP. The negative anomaly in the north extends eastward and then moves southward in the eastern Pacific. The positive anomaly in the south, which can be traced back to the central midlatitudes in the 1970s, moves westward in the subtropics. About a decade later, this positive anomaly has moved across the subtropics and then northward. Note that the spatial structure of temperature anomalies in 1990 (Fig. 2f) is similar to that in 1974 (Fig. 2b) but with reversed polarity. It appears that the positive and negative anomaly patterns rotate around the subtropical gyre, suggesting a cycle that circulates clockwise in the entire North Pacific Ocean.

Figure 5 shows temperature anomalies as a function of depth and time from four different typical regions at (a) 22.5°N and 162.5°E–132.5°W, (b) 27.5°N and 145.5°E, (c) 42.5°N and 177.5°–155.5°W, (d) 27.5°N and 127°W, respectively. Decadal variations and structural differences in the horizontal as well as in the vertical can be clearly seen. The maximum temperature anomalies appear at subsurface depths, not at the sea surface. There are phase differences in the temperature variations in the east and in the west, at the sea surface and at depth, as well as in the midlatitudes and in the subtropics. In particular, temperature changes tend to be out-of-phase in the central midlatitudes and the North American coast (Figs. 5–d). In addition, Fig. 5 also suggests a movement of temperature anomalies from the subtropical Pacific Ocean (Fig. 5a) to the Kuroshio region (Fig. 5b), to central midlatitudes (Fig. 5c), and to the coast of North America (Fig. 5d). The phase patterns suggest a cycle, with anomalies circulating clockwise in succession: westward in the subtropics, northward in the western boundaries, eastward in the midlatitudes, and equatorward in the east.

These findings are based on analyses of the observed historical temperature profiles and minimal processing has been applied to the data displayed here. These basic results will be further demonstrated in the following sections using more elaborate analyses. Such a cycle has been suggested by Latif and Barnett (1994, 1996) based on output from a coupled ocean–atmosphere model.

4. Principal structure at upper-ocean standard levels

Section 3 provided basic descriptions of some features of the decadal variations in the temperature of the upper North Pacific Ocean. To detect the dominant structure and their time variations, we perform an empirical orthogonal function (EOF) analysis for temperature anomaly fields at all standard oceanographic levels from the sea surface to 400-m depth. The horizontal domain of our analysis is the 7.5°N to 62.5°N region of the North Pacific Ocean. The EOFs are computed based on a covariance matrix for the 30 yr of annual fields for 1961 to 1990. Table 1 presents percent variances explained by the first four EOF modes for each level. Examples are given in Figs. 6–7 to show the spatial patterns and time variations of the first two EOFs modes for temperature at the sea surface and 250-m depth, respectively.

The spatial pattern (Fig. 6b) and its time series (solid line in Fig. 6a) for the first EOF of SST are similar to other previous studies (Watanabe and Mizuno 1992; Tanimoto et al. 1993; Levitus et al. 1994b; Kawamura 1994). This mode, which accounts for 33.9% of total variance, has a large amplitude in the western and central midlatitude North Pacific and along the Northern American coast region. The second eigenvector (Fig. 6c) shows a positive anomaly region in the midlatitudes and in the subtropical eastern Pacific. Thus, the positive anomaly covers a larger portion of the northern and subtropical Pacific Ocean, with negative anomalies in the northern North Pacific and in the subtropical central region.

The EOF time coefficients of the amplitude for SST indicate the decade-scale variations (Fig. 6a). In particular, the first EOF (Fig. 6a) shows a warming period between 1968 and 1974. In the mid-1970s the multiyear warm state terminates and there is a sharp transition to a cold condition, with SST cooling in the central midlatitudes but warming off the coast of western North America (Fig. 6a). The time series of the second EOF mode also shows decadal variations.

Figures 7b–c show the principal structure of the de-

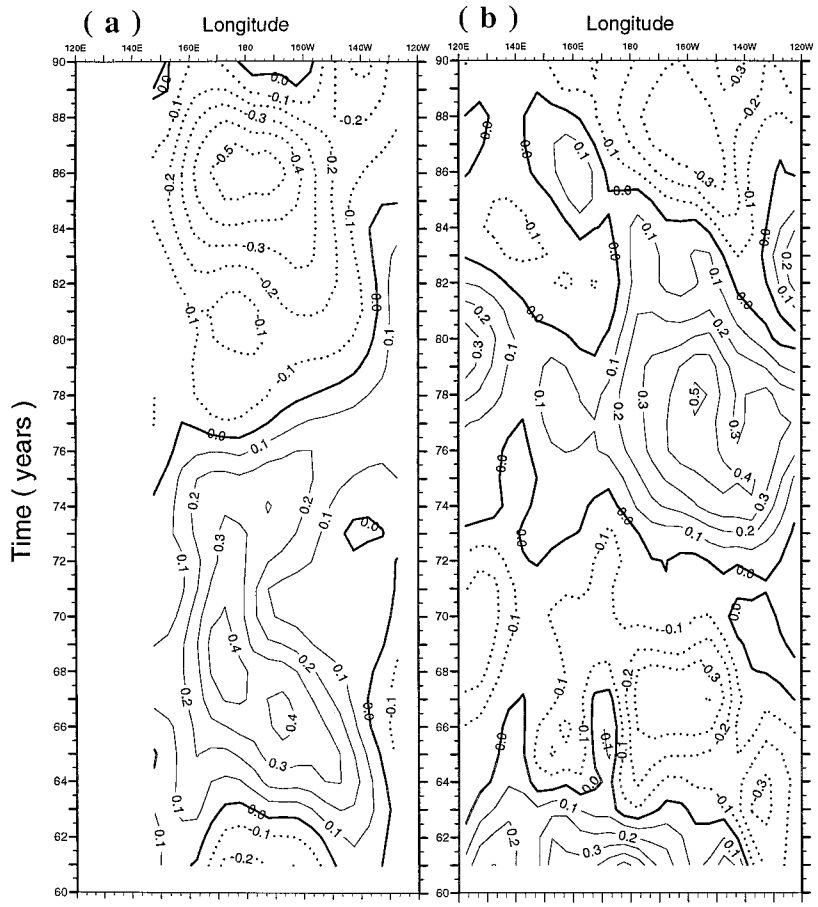

FIG. 2. Decadal variations in temperature at 250-m depth in longitudes along (a) 42.5°N and along (b) 22.5°N, and in latitudes along (c) 162.5°E, and along (d) 142.5°W, respectively. The contour interval is 0.1°C with a dotted line representing negative values.

cadal temperature variability at 250-m depth. The spatial patterns at this depth are basically similar to those at the sea surface, but with spatial displacement of the anomaly maxima. The first mode (Fig. 7b) depicts an east–west oriented dipole pattern, characterized by opposite phase in the midlatitudes and in the subtropics. When one positive center is located in the north, a negative anomaly band tends to be located in the subtropical region. While the negative anomaly maxima tend to take place in the North American coastal region at the sea surface, those at 250-m depth are located in the subtropics of the ocean interiors. The second eigenvector (Fig. 7c) indicates a pattern of opposite sign in changes of temperature from the western Pacific along 30°N (a narrow positive band) to broad central and eastern Pacific regions.

Figure 7a presents the corresponding time variations of the first two EOFs at 250-m depth. These variations coincide with those at upper depths, but also clearly show a phase shift of the decadal temperature variability at different ocean depths. In addition, these two time series indicate a clear phase relation with the EOF2 leading EOF1. This suggests that the spatial patterns associated with EOF2 (Fig. 7c) will appear first and then those associated with EOF1 (Fig. 7b) appear. Examination of the spatial distributions of the second (Fig. 7c) and first (Fig. 7b) eigenvectors indeed demonstrates such a phase movement of anomaly patterns around the subtropical gyre. The negative anomaly in the central midlatitude northern and eastern Pacific depicted by the second EOF mode (Fig. 7c) is found to be located in the subtropics as described by the first EOF mode (Fig. 7b); the positive anomaly in the western Pacific along 30°N revealed by the second mode (Fig. 7c) is located in the western and central midlatitudes as depicted by the first EOF mode (Fig. 7b). This is suggestive of a subsurface thermal cycle, which circulates clockwise on a basin scale in the North Pacific Ocean. The regression analysis (section 6) will demonstrate this feature more clearly.

5. Combined structure

The EOF analyses in section 4 performed separately on each level clearly show the structural and phase dif-

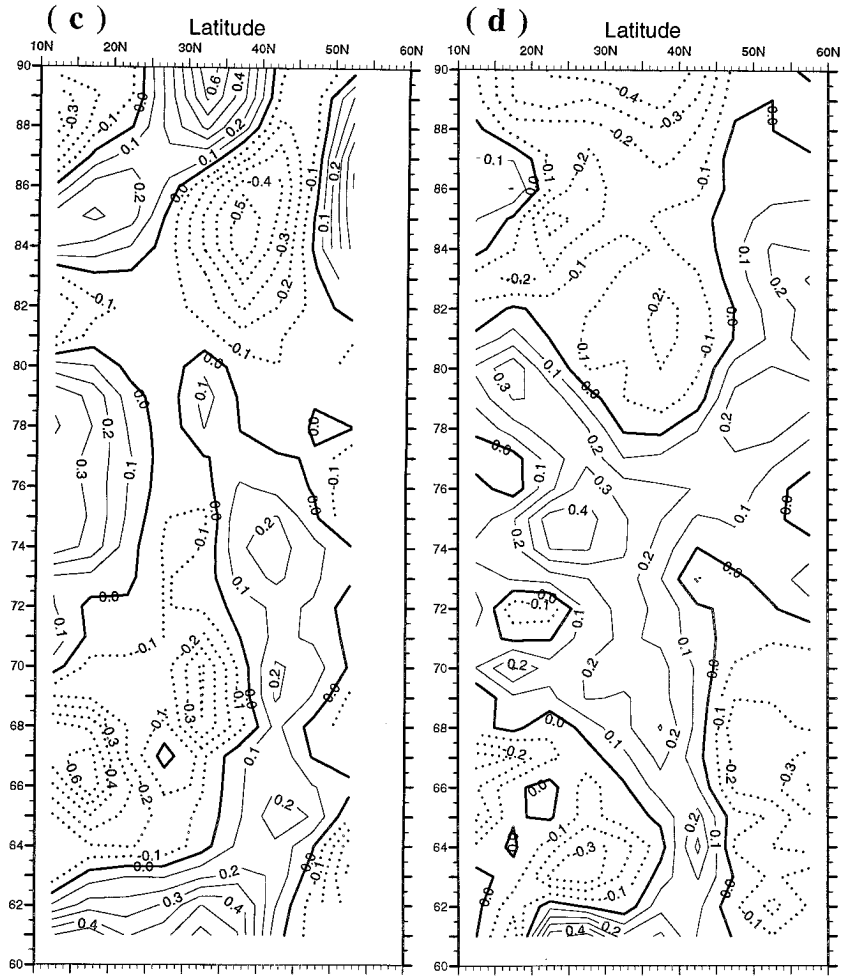

FIG. 2. (*Continued*)

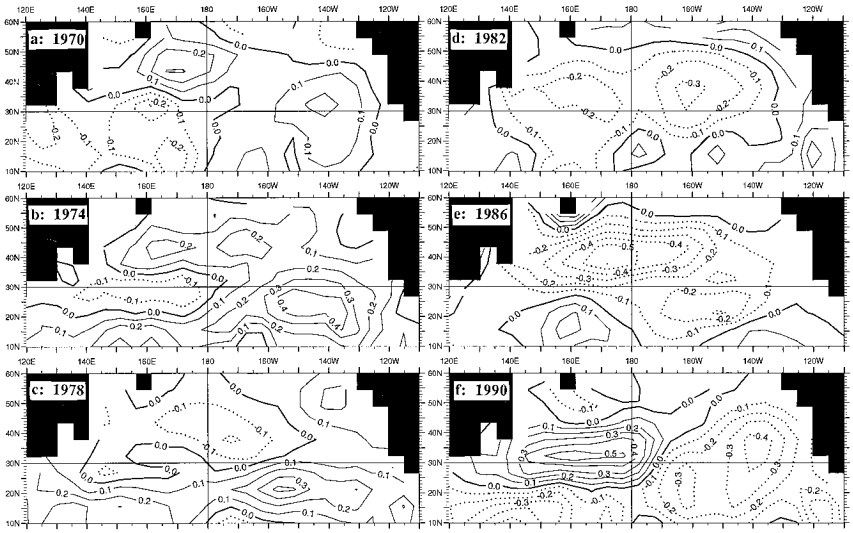

FIG. 3. Horizontal distribution of temperature anomalies at 250-m depth in the North Pacific Ocean for year (a) 1970, (b) 1974, (c) 1978, (d) 1982, (e) 1986, and (f) 1990, respectively. The contour interval is 0.1°C with a dotted line representing negative values.

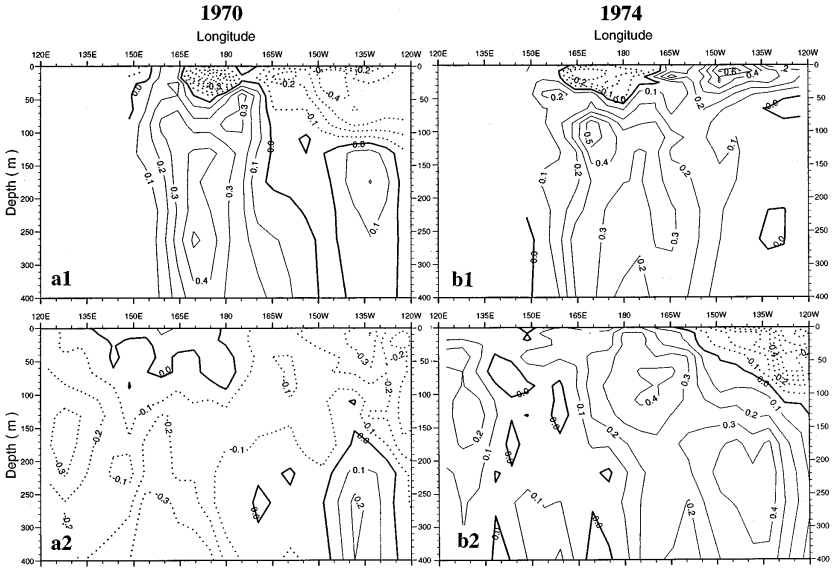

FIG. 4. Longitude–depth sections of temperature anomalies along 42.5°N (upper panel) and 22.5°N (lower panel) for year (a) 1970, (b) 1974, (c) 1978, (d) 1982, (e) 1986, and (f) 1990, respectively. The contour interval is 0.1°C with a dotted line representing negative values.

ferences in the temperature variations at the sea surface and at depths. To provide information on any vertically coherent three-dimensional anomaly structure, a combined EOF analysis is performed simultaneously on the temperature anomaly fields at depths of 0, 10, 20, 30, 50, 75, 100, 125, 150, 200, 250, 300, and 400 m of the North Pacific Ocean between 7.5° and 62.5°N.

The first four combined EOFs explain about 27%, 17%, 11%, and 10%, respectively, of the total variance (Table 1). Figure 8 depicts the time series of the amplitude for the first two combined EOF modes. It is apparent that the quasi-decadal variations are present. The first mode has a maximum amplitude in the early 1970s and the middle 1980s. During the late 1970s, this mode clearly shows the 1976–77 climate transition in the North Pacific Ocean, from a warm to a cold state. The second EOF mode has a maximum amplitude around 1975 and reflects a transition state from DWP to DCP. Since these two EOF time series appear approximately in quadrature with EOF 1 lagging EOF 2, a phase propagation phenomenon is suggested. Thus, the spatial patterns associated with the second EOF mode (Fig. 9) will appear first and then those associated with the first EOF mode (Fig. 10) appear. In keeping

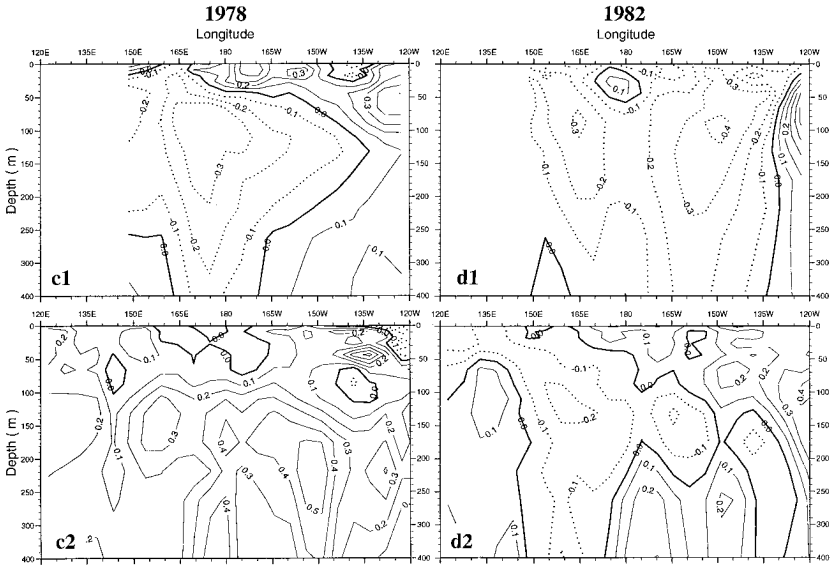

FIG. 4. (*Continued*)

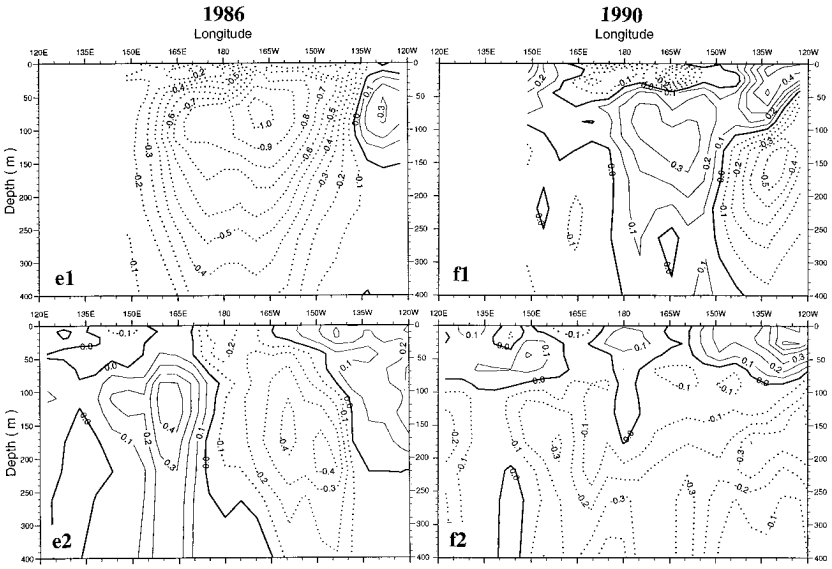

FIG. 4. (*Continued*)

with this chronology, EOF 2 will be shown and described first as follows.

Figure 9 shows the spatial patterns of the second combined EOF modes for temperature at the sea surface, 125-, 250-, and 400-m depths, respectively. There is a good correspondence between the spatial pattern of the second eigenvector depicted by the combined EOF analyses and those from the individual EOF analyses at each ocean level (section 4). As shown in Fig. 9, SST has large positive amplitude in the eastern Pacific, with a corresponding negative pattern in the central midlatitudes. This is sharply contrasted to temperature anomalies at the subsurface depths (Figs. 9b–d), indicating phase differences between the decadal temperature variability in the vertical. At subsurface depths, negative anomalies are located in the subtropical Pacific and the North American coastal region, with the largest amplitude in the western and central subtropics. This is accompanied by a positive anomaly band in the Kuroshio and its extension region, with southwest–northeast-oriented direction.

After about 5 yr, the spatial patterns are described by the first mode (Fig. 10). There is a dominant positive anomaly region in the western and central midlatitude

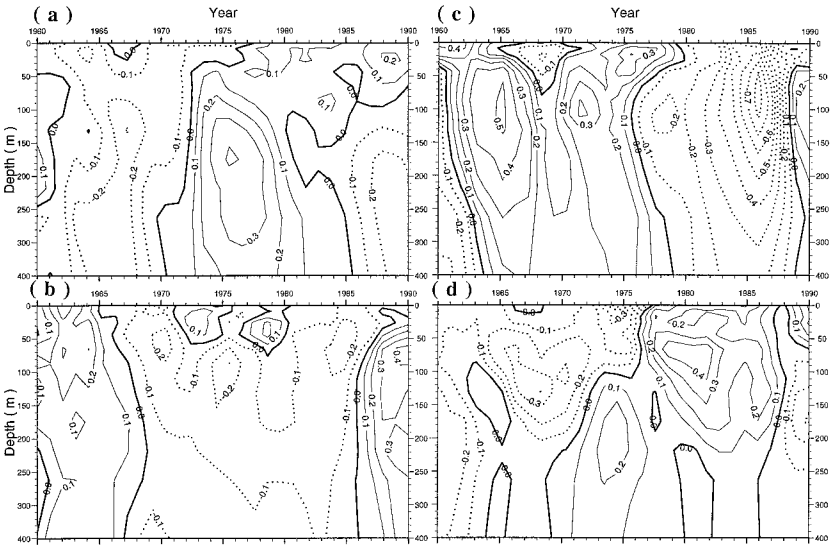

FIG. 5. Temperature anomalies as a function of depth and time at (a) 22.5°N and 162.5°E–132.5°W, (b) 27.5°N and 145.5°E, (c) 42.5°N and 177.5°–155.5°W, (d) 27.5°N and 127°W, respectively. The contour interval is 0.1°C with a dotted line representing negative values.

TABLE 1. Fractional variances for each level explained by the first four EOF modes. The results for the combined EOF analysis performed on whole upper ocean is also given.

Depth	Modes (%)				Cumulative (%)
	EOF-1	EOF-2	EOF-3	EOF-4	
0	33.9	14.0	12.2	6.8	66.9
10	29.6	18.5	10.6	7.6	66.3
20	31.9	17.0	11.3	7.9	68.1
30	31.8	16.2	10.8	8.0	66.8
50	31.8	16.2	10.9	9.6	68.5
75	33.3	12.3	11.2	8.7	65.5
100	37.6	11.3	10.2	8.4	67.5
125	35.1	16.6	10.6	9.0	71.3
150	29.7	20.9	10.8	8.7	70.1
200	28.2	23.7	12.1	6.9	70.9
250	30.9	20.0	14.3	8.1	73.3
300	31.8	23.8	14.4	5.7	75.7
400	31.7	24.4	11.3	10.0	77.4
Mean	32.1	18.1	11.6	8.1	69.7
Combined EOF	26.6	17.1	11.3	9.6	64.6

North Pacific, surrounded by a negative anomaly in the subtropics and in the North American coast region. The temporal relation between the first two EOF time series (Fig. 8) and the spatial patterns of the first two EOF modes (Figs. 9–10) suggest a cyclic phase movement in a clockwise sense around the subtropical gyre of the North Pacific Ocean, as mentioned in section 4.

Figure 11 shows the longitude–depth structure of the first two combined EOF modes along 42.5°N and along 22.5°N, respectively. The second EOF mode (Figs. 11a–b) depicts the contrast of temperature variation between the midlatitudes and the subtropics. Also it is evident that temperature variations in the surface layer tend to be opposite to those at subsurface depths in the central midlatitudes and in the eastern subtropical Pacific (i.e., baroclinic structure). The first EOF mode shows dominant positive anomalies in the midlatitudes, with the maximum located at 100-m depth. This is accompanied by a corresponding negative anomaly along the Northern American coast and in the subtropical Pacific.

6. Space–time evolution

The previous two sections presented the most important modes of the decadal temperature variability in the North Pacific Ocean. In this section we will examine the typical space–time evolution of temperature anomalies during a decadal cycle.

To describe the time evolution, we perform linear regression pattern analysis on the upper-ocean temperature anomaly fields. The temporal coefficients of the first combined EOF (solid line in Fig. 8) are chosen for defining the time evolution of decadal variability. Temporal regression coefficients are computed between this reference time and the temperature anomalies at individual grid points for different time lags, thus providing a basinwide three-dimensional picture associated with the decadal cycle. Figures 12–13 demonstrate a sequence of events at the sea surface and at 250-m depth with 4-yr time intervals. Figure 14 exhibits longitude–depth sections of regression patterns along 42.5°N and 22.5°N, respectively. All charts at zero lag are very similar to the corresponding spatial distribution of the first combined EOF mode (Fig. 10 and Figs. 11c–d) and therefore are omitted. The panels have been arranged in the order of increasing time lags so that evolution can be seen clearly. For example Fig. 14a illustrates the spatial structure for the reference time lagging the temperature data by 2 yr, and Fig. 14b shows that for the reference time leading the data by 2 yr. In this way, the space–time evolution of temperature anomaly can be revealed.

Figure 12 shows the regression patterns between SST and the first combined principal component at lag -10, lag -6, lag -2, lag $+2$, lag $+6$, and lag $+10$ yr, respectively. Note that the spatial structure at lag -6 yr (Fig. 12) corresponds well to that of the second combined EOF mode (Fig. 9a). Spatial patterns at lag -2 and lag $+2$ years are similar to those of the first combined EOF mode (Fig. 10a). Although there is a clear spatial pattern at the peak of DWP or DCP, it is difficult to see a consistent and coherent pattern of the space–time evolution and phase movement of the SST anomalies.

At 250-m depth (Fig. 13), the space–time evolution appears to be well-organized. A coherent pattern, rotating around the subtropical gyre, is evident, consistent with the finding about the time sequence of temperature changes described above. At lag -10 yr the spatial patterns are similar to the second EOF eigenvector (Fig. 9c). There is a positive anomaly band along the Kuroshio and its extension region, but a negative anomaly in the subtropical eastern Pacific. These anomaly patterns appear to continue their phase movement in the entire North Pacific Ocean on a decadal timescale. After 4 yr, the positive temperature anomaly has extended into the midlatitudes and the negative anomaly propagates westward in the subtropics. Four years later (Fig. 13c), the positive anomaly has intensified while the negative anomaly has moved across the basin. Subsequently, these anomaly patterns seem to rotate clockwise around the subtropical gyre. The positive band at midlatitudes has circulated in the central and eastern Pacific to the subtropics whereas the negative anomaly moves westward and northward in the western Pacific. At lag $+10$ yr (Fig. 13f), the positive anomaly is located in the subtropical region, while the negative anomaly is found in the Kuroshio Extension region. The spatial structure is very similar to that at lag -10 yr but with reverse polarity in anomaly, representing the completion of one cycle.

The three-dimensional structure and evolution of upper-ocean temperature anomalies are further demonstrated in Fig. 14, which shows longitude–depth sections of the regression coefficients along 42.5°N and along

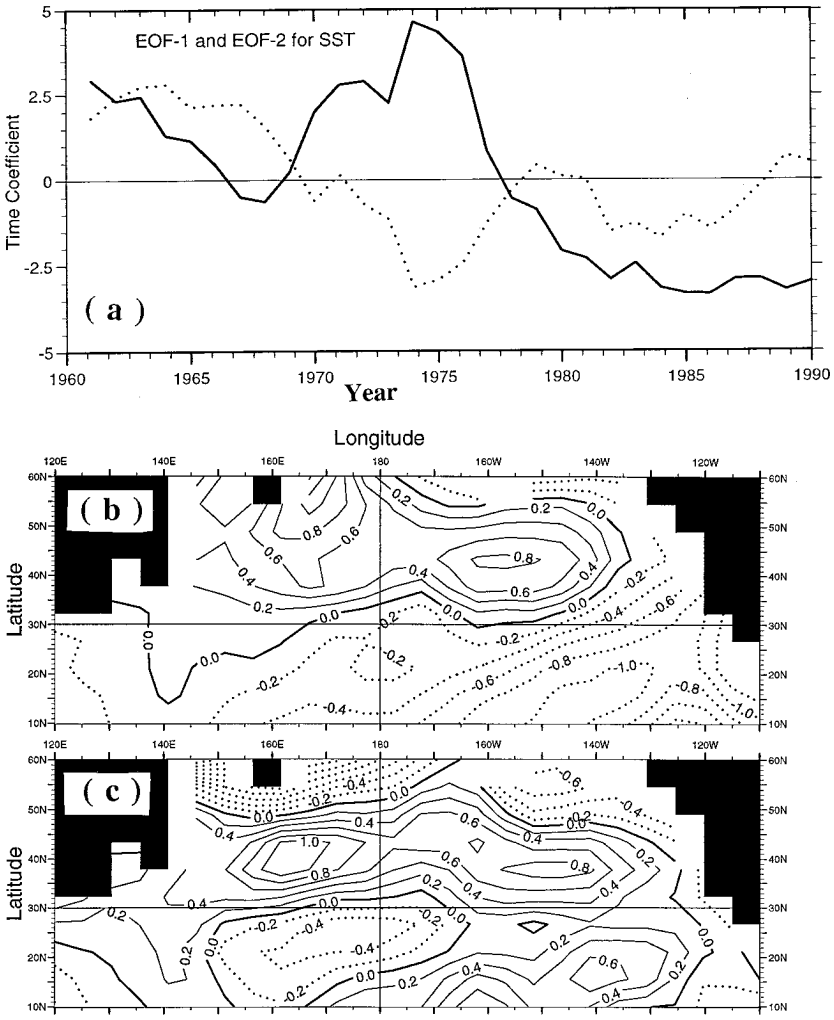

FIG. 6. Time variations and spatial pattern of the first two EOF modes for SST. (a) The solid line for the first mode and the dotted line for the second one; (b) The first eigenvector; (c) the second eigenvector. Contours in (b) and (c) show the actual eigenvector value multiplied by 10. The contour interval is 0.2 with a dotted line representing negative values.

22.5°N at different time lags. Figures for lag −10 and lag −6 yr (not shown) correspond well to those from the second combined EOF analysis (Figs. 11a–b). There is an out-of-phase anomaly pattern in latitudes at midlatitudes and in the subtropics where a dominant negative anomaly is observed at subsurface depths. At lag −2 yr (Fig. 14a), the basic spatial structure remains unchanged, with a weakening of the negative anomaly in the subtropics but a strengthening of the positive anomaly in the central midlatitudes. To zero lag yr (figures not shown but very similar to Figs. 11c–d from the first combined EOF analysis), the positive anomaly in the midlatitudes has been largely stationary with a significant increase in the amplitude. The negative anomaly in the subtropics, on the other hand, has been moving across the basin to the western Pacific. At lag +2 yr (Fig. 14b), a striking feature is an appearance of a positive subsurface anomaly in the subtropical eastern Pacific. The subsequent evolution of temperature anomalies suggests a clockwise movement of the subsurface patterns around the subtropical gyre. Along 22.5°N, the subsurface positive anomaly amplifies and shows westward zonal propagation in longitude across the subtropics. Along 42.5°N, on the other hand, the positive temperature anomaly weakens and moves eastward and southward (Fig. 14c). In the western Pacific, the negative anomaly, which has propagated across the subtropics from east to west, moves northward along the boundary region. At lag +8 yr (Fig. 14d), the negative temperature anomaly appears in the Kuroshio region and warm conditions in the midlatitudes decay significantly. At lag +10 and lag +12 yr (Figs. 14e–f), temperature anomalies are negative in the central midlatitudes but positive at the subsurface depths of the subtropical Pacific Ocean, thus reversing anomaly phase in the north and in the south. The subsequent evolution follows the

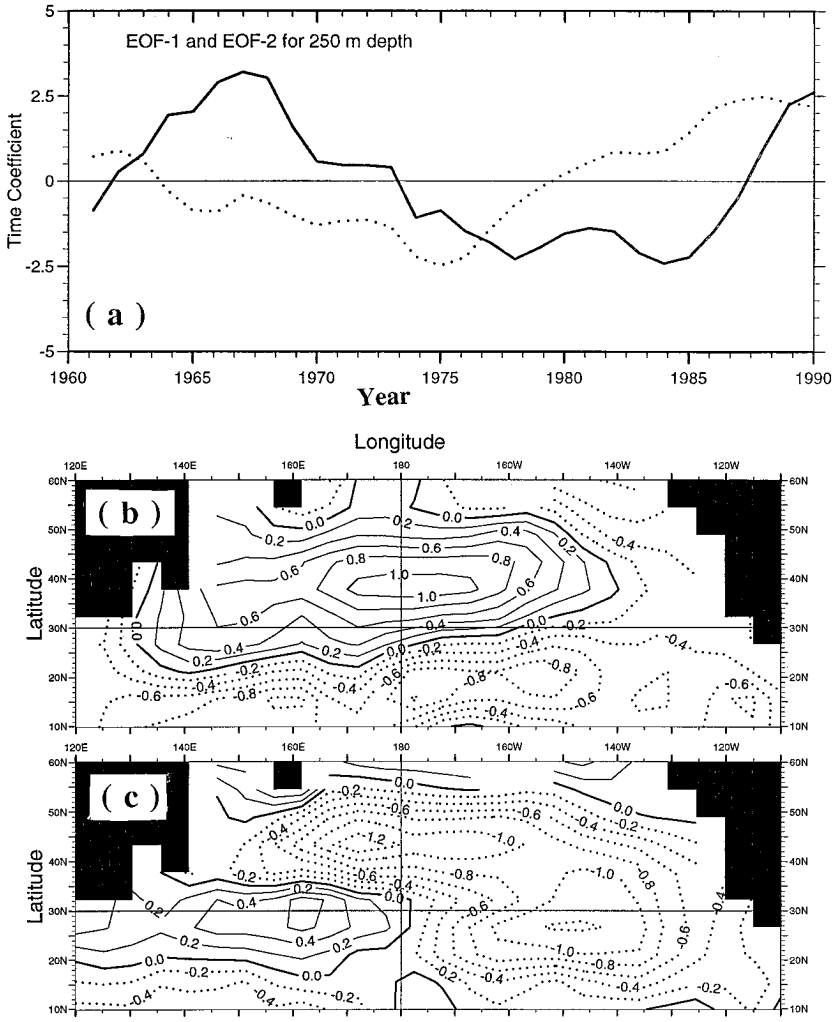

FIG. 7. The same as in Fig. 6 but for temperature at 250-m depth.

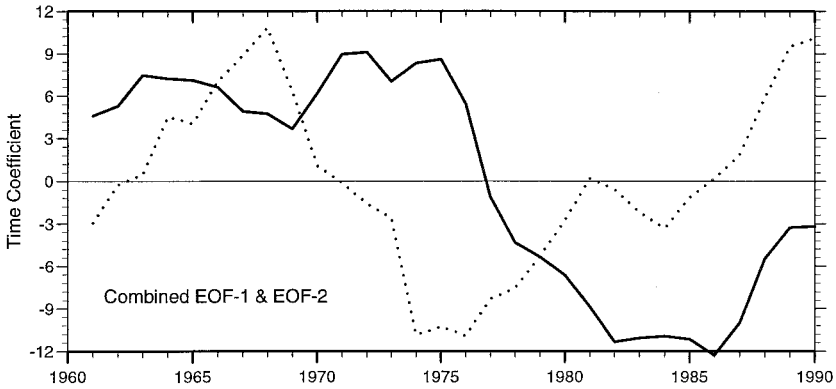

FIG. 8. Time variations of the first (solid line) and the second (dotted line) coefficients of the combined temperature EOF modes.

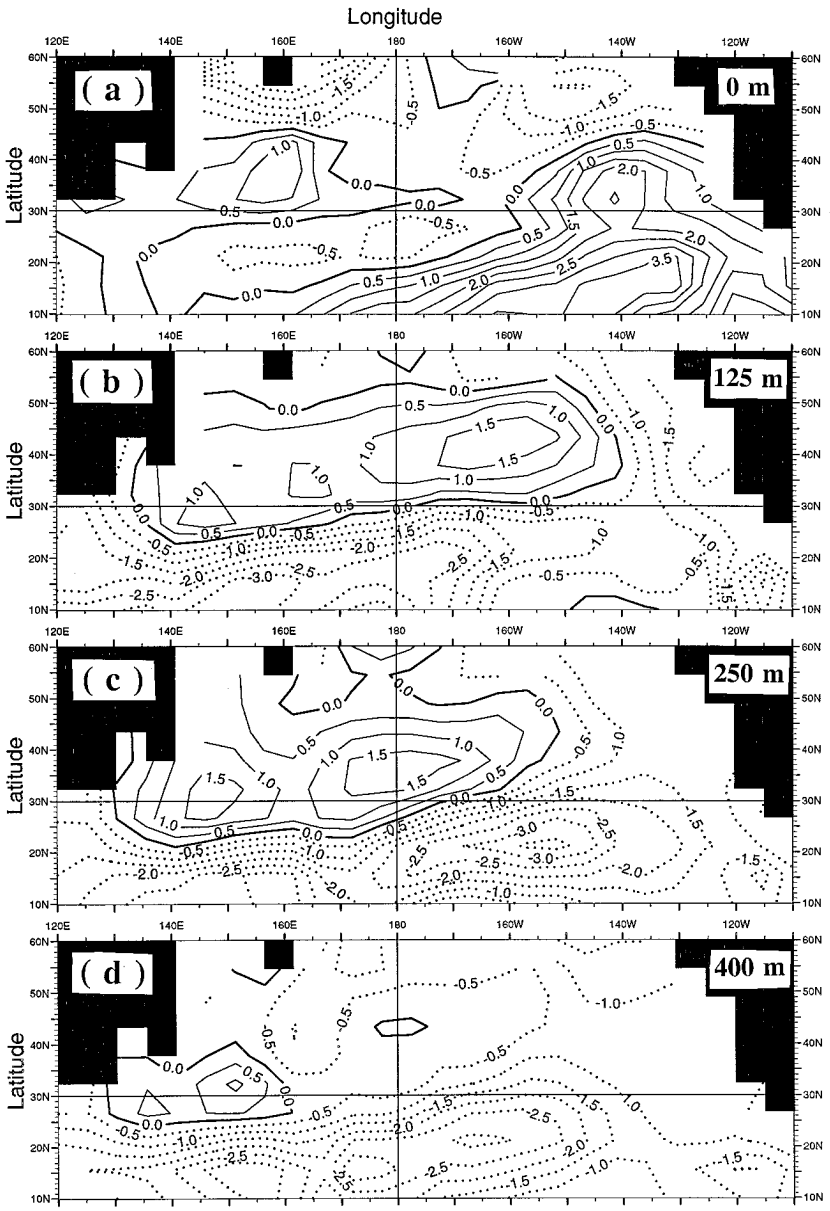

FIG. 9. Spatial pattern of the second combined EOF mode for temperature at (a) sea surface, and at (b) 125-m, (c) 250-m, and (d) 400-m depths, respectively. Contours in these figures show the actual value multiplied by 100. The contour interval is 0.5 with a dotted line representing negative values.

same route but with opposite polarity and begins another cycle.

7. Summary and discussion

We described the three-dimensional structure and evolution of decadal variability in the North Pacific based on observed upper-ocean temperature data from 1961 to 1990. The decadal variability cycle is revealed by using regression analysis between the temporal coefficients of the first combined EOF mode and the temperature anomaly fields. The analyses detect the principal basin-scale structure of decadal-scale warm period (DWP) and cold period (DCP). There is a well-defined subsurface thermal pattern, characterized by a prominent see-saw structure with opposite anomaly polarity between the midlatitude North Pacific and the subtropics. During the DWP, a positive temperature anomaly is found in the central midlatitude upper ocean with a maximum at about 100-m depth. This is accompanied by a corresponding negative anomaly in the American coastal region and in the subtropics. In addition to the

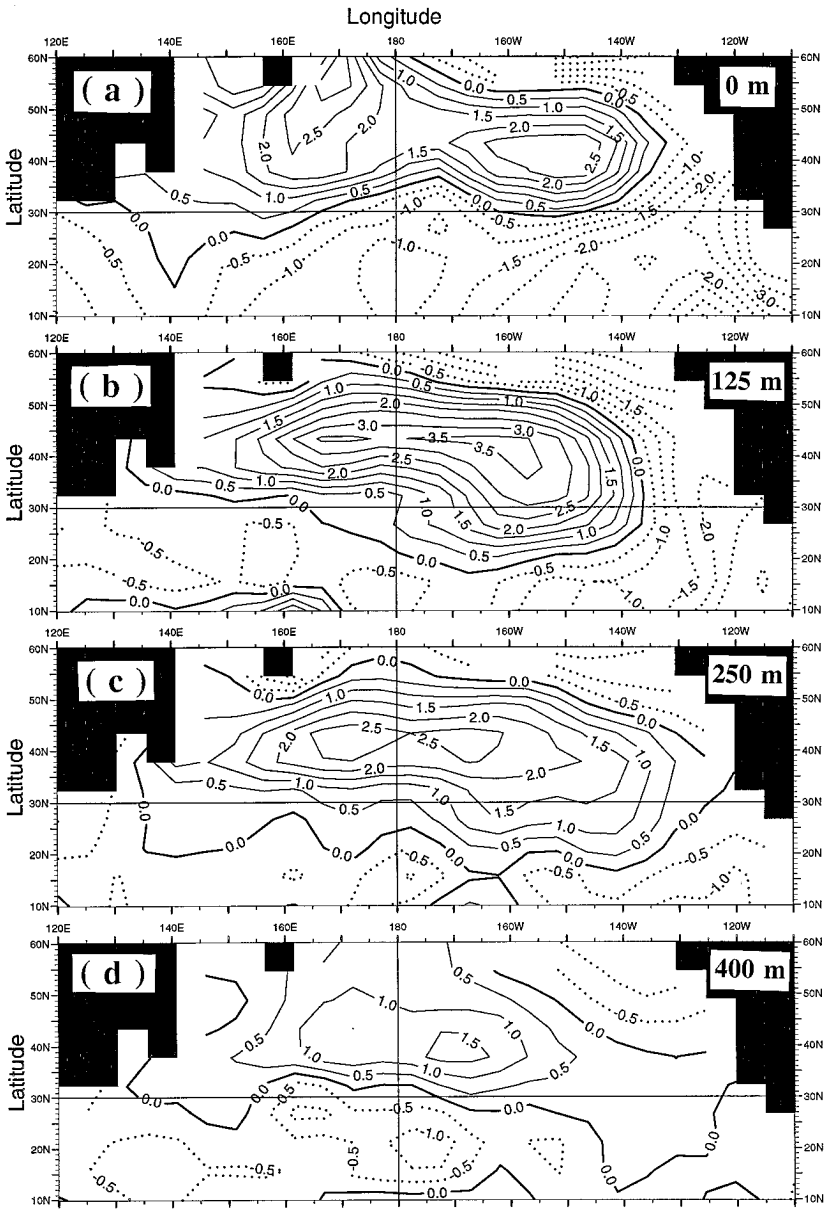

FIG. 10. The same as in Fig. 9 but for the first combined EOF mode.

east–west seesaw pattern in the central midlatitudes and off the North American coast, an east–west-oriented dipole structure in the midlatitudes and the subtropics is more evident at 50–200-m depths than that at the sea surface. When a positive anomaly occurs at midlatitudes, a negative anomaly tends to occur at the subsurface depths of the subtropical Pacific. A reverse pattern of these anomaly is observed during the DCP.

Evolution between DWP and DCP involves systematic zonal and meridional transfers of anomaly phase in the entire North Pacific Ocean, showing consistent and coherent variations from subsurface to sea surface, from central midlatitudes to North American coastal regions, and to subtropics. Temperature anomalies appear to circulate around the subtropical gyre in the North Pacific. This phase propagation is evident at subsurface depths but not at the sea surface; propagation is westward in the subtropics but eastward in the midlatitudes. In addition, there are structural and phase differences between temperature changes at the sea surface and at subsurface depths. The subtropical subsurface ocean is shown to be an important region in the decadal variability cycle, characterized by systematic and coherent westward trans-Pacific phase propagation.

The basinwide structure and time evolution of the decadal subsurface temperature variability in the North Pacific Ocean are described in the present paper based solely on observational data. Such basin-scale evolution

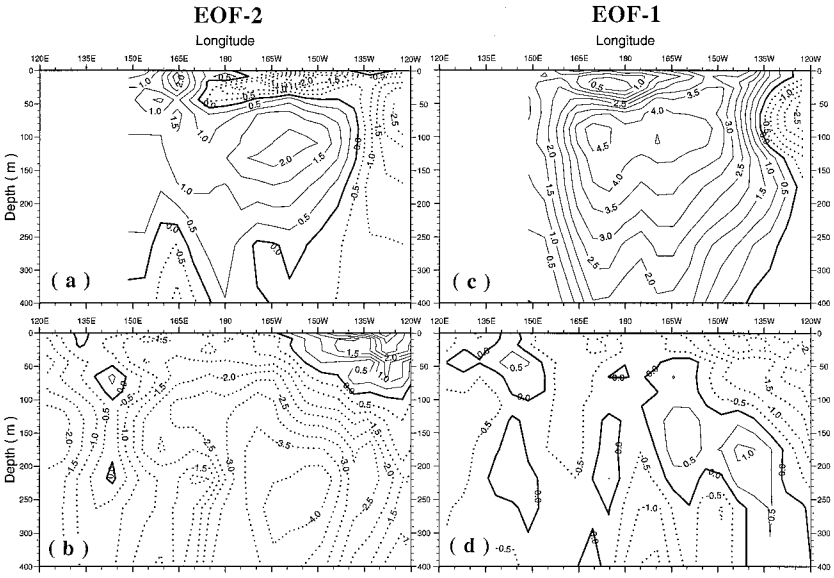

FIG. 11. Longitude–depth sections of the second (left) and first (right) combined EOF modes along 42.5°N (upper panel) and along 22.5°N (low panel), respectively.

in the ocean suggests that the ocean may play an active role in the existence of decadal variability in the North Pacific climate system. Evolution of the subsurface temperature anomaly fields appear to be in the form of a cycle that circulates clockwise around the subtropical gyre. During a decadal warm phase, which is characterized by high temperature in the central midlatitude upper ocean, the seeds for a decadal cold phase seem to be present to the south at the subtropical subsurface depths, where there occurs a negative anomaly which, in turn, can be traced back further to the eastern North Pacific. Evolution between DWP and DCP is characterized by zonal and meridional propagation of anomaly phase in the entire North Pacific. The westward trans-Pacific propagation of the subsurface negative temperature anomalies in the subtropics is a striking feature and provides negative anomaly source for the western Pacific. Subsequently, cold subsurface waters expand northward in the west and move eastward along the Kuroshio and its extension region. Their arrival causes the termination of the warm conditions in the central midlatitudes and then cold conditions prevail thereafter.

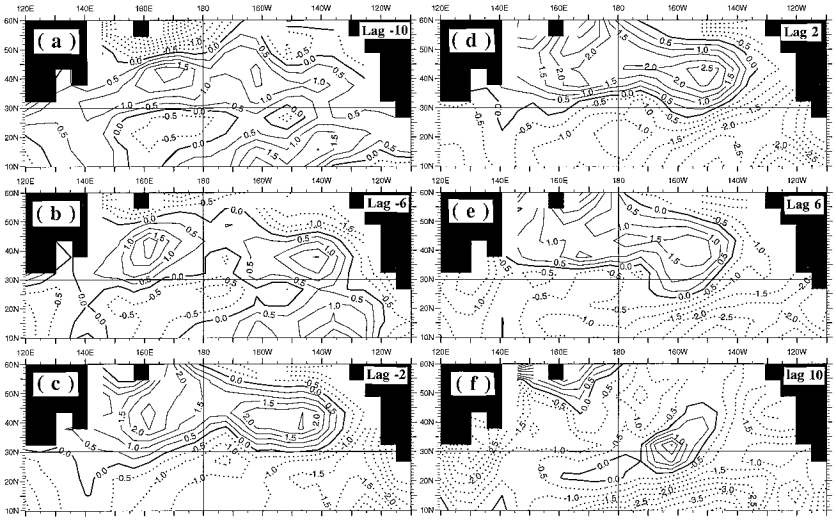

FIG. 12. Regression patterns between the first combined principal component (solid line in Fig. 8) and SST anomalies for (a) lag −10 yr, (b) lag −6 yr, (c) lag −2 yr, (d) lag +2, (e) lag +6, and for (f) lag +10 yr, respectively. Contours in these figures show the actual value multiplied by 100. The contour interval is 0.5 with a dotted line representing negative values.

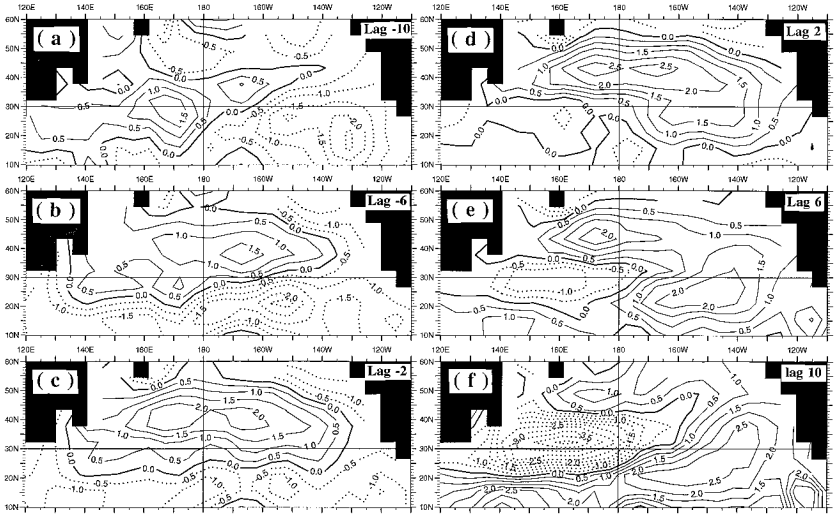

FIG. 13. The same as in Fig. 12 but for temperature at 250-m depth.

At the same time, there appears a positive temperature anomaly at subsurface depths in the subtropical Pacific. The evolution from DCP to DWP follows the same route but with the reversal polarity, thus forming a cycle. Note that, unlike temperature variations at subsurface depths, SSTs do not show consistent and coherent phase movements in the subtropics. The continual movement of subsurface temperature anomaly on decadal timescale around the subtropical gyre suggests a phase-switching mechanism. This subsurface cyclic process may contribute to establishing SST variations in the midlatitude North Pacific, which, in turn, influences the atmospheric circulation, thus providing a decadal-scale memory mechanism. Furthermore, such subsurface ocean memory may maintain the self-sustained quasi-decadal variability for the coupled climate system in mid- and high latitudes. In addition, it is such subsurface ocean memory that may provide a physical basis for prediction of decadal climate variability. It seems, therefore, that the subsurface ocean plays an important role in generating and maintaining decadal variability of the coupled climate system over the North Pacific.

Recently, numerical simulations have been one of the most powerful tools for describing, understanding, and

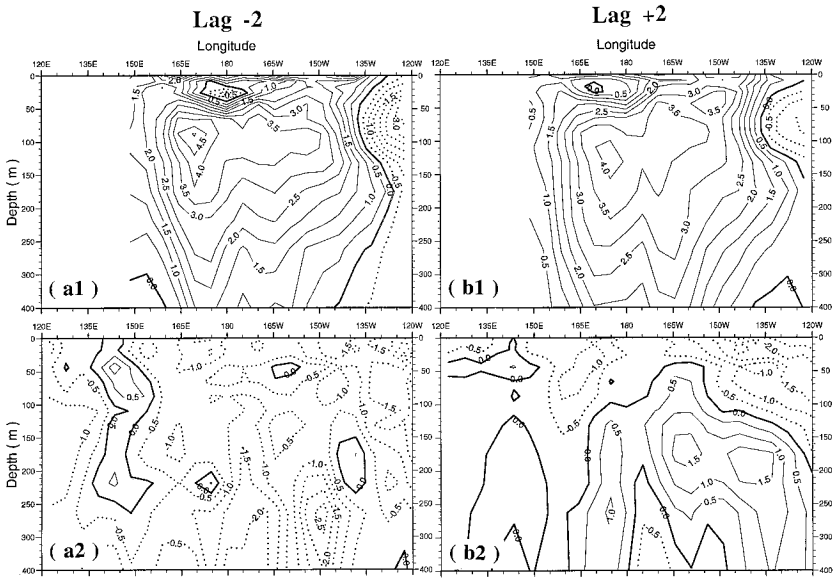

FIG. 14. Longitude–depth sections of regression patterns between the first combined principal component (solid line in Fig. 8) and upper-ocean temperature anomalies along 42.5°N (upper panel) and along 22.5°N (low panel) for (a) lag −2 yr, (b) lag +2 yr, (c) lag +6 yr, (d) lag +8 yr, (e) lag +10 yr, and for (f) lag +12 yr, respectively.

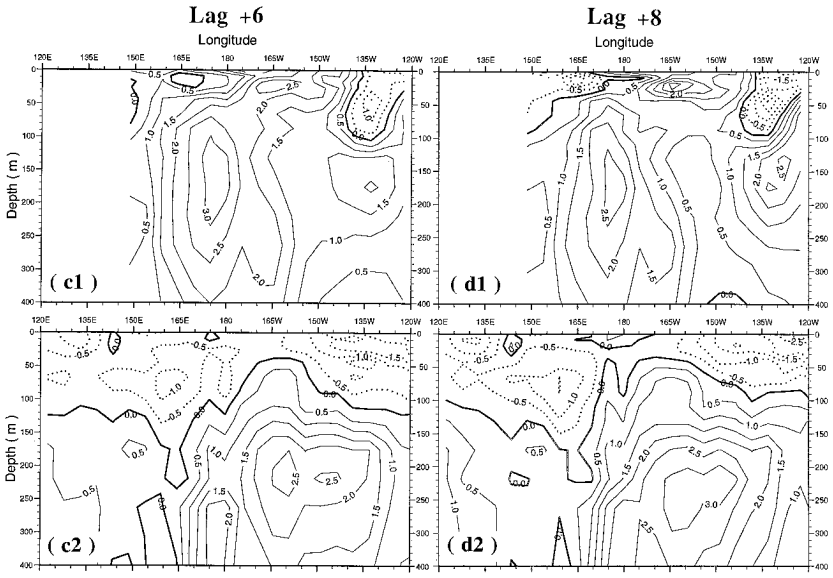

FIG. 14. (*Continued*)

predicting decadal variability of the coupled atmosphere–ocean climate system. Several ocean and coupled atmosphere–ocean models have been developed with ability to produce some decadal-scale variability feature in the Pacific, but they differ strikingly from each other (Miller et al. 1994a,b; von Storch 1994; Graham 1994; Latif and Barnett 1994, 1996). The decadal thermal variability in the North Pacific Ocean found by Latif and Barnett (1994, 1996) from a coupled air–sea model bears a close resemblance to our results, such as the structure and evolution of the subsurface thermal pattern characterized by a clockwise rotating cycle, and the characteristic timescale (about 20 yr). This suggests that the model realistically represents the fundamental physics of decadal-scale climate variability in the system. There are, however, some interesting features that need to be examined further in the model-data comparison studies. The space–time evolution from the data indicates a prominent westward trans-Pacific phase propagation (in the form of a planetary wave) all the way across the subtropical Pacific region, whereas at midlatitudes other signals, such as a forced response by the overlying atmosphere and thermodynamically induced variations, are more apparent so that the decadal variability in this region is more likely dominated by a standing pattern. The data indicate that the clockwise

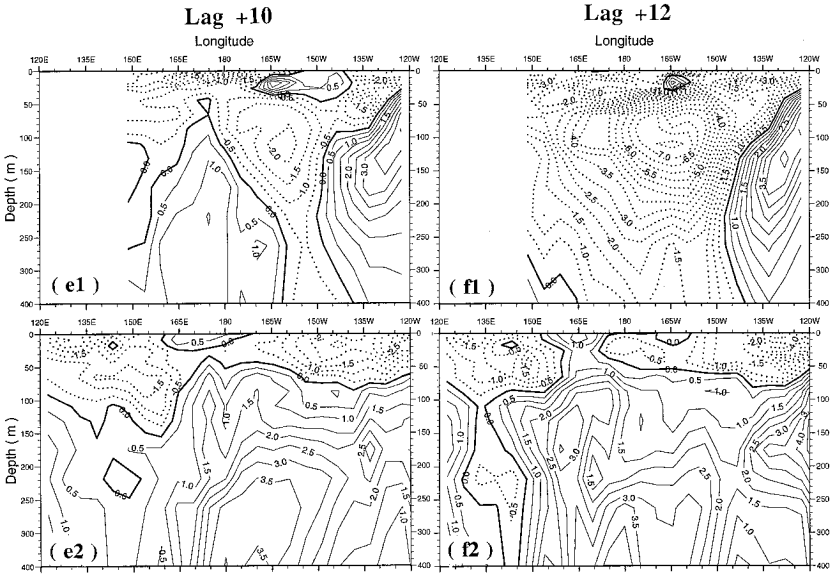

FIG. 14. (*Continued*)

rotation speed is not uniform around the subtropical gyre, much faster in the subtropical western boundary and the Kuroshio regions than in the midlatitude ocean interiors where the anomaly movement seems to stall at times. There is a strong tendency for a rotating thermal anomaly to decrease in extent and strength when moving through the western subtropical Pacific but to amplify considerably in the magnitude and to extend in dimension (both in the vertical and horizontal) when moving into the midlatitude North Pacific Ocean. The baroclinic structure of the decadal temperature variability is evident particularly in the subtropical and the Kuroshio regions where there are significant phase differences in the vertical between the sea surface and subsurface depth. The other ocean or coupled models seem to have problems to realistically produce the subsurface phase propagation all the way across the subtropical Pacific basin, which, as discussed above and explained by Latif and Barnett (1994, 1996), reflects a nonequilibrium adjustment in the ocean and provides a phase transition mechanism for decadal-scale oscillation. In addition, some models underestimate or even lack the important phase differences in decadal-scale thermal variations at the sea surface and at subsurface depths. Instead, the decadal variations are predominated by thermodynamical processes related to local interactions between atmosphere and ocean, and between the surface mixed layer and the thermocline. Hence, it is not surprising that, without a phase-switching mechanism provided by subsurface ocean dynamics, the model behavior of decadal variability will be strikingly different. Thus, the models need to be improved. The results presented in the paper, therefore, provide observational evidence for the space–time evolution of the subsurface ocean thermal structure in the North Pacific Ocean.

Further extension of the results presented in this work is desirable in several aspects. Because of data sampling limitations (e.g., yearly composites of temperature data), a detailed description of the space–time evolution in a seasonal sequence is still necessary when more data become available on a monthly basis. This is especially important because of the strong dependence of decadal variability on the season as noted by Deser et al. (1996). Although the data offer a possibility of describing observational structure and evolution of decadal variability in the North Pacific, the 30-yr record is obviously not long enough to establish a statistical significance of a mode with about a 20-yr period in the region. Thus, the inferred cycle characterized by the clockwise rotation of the subsurface thermal pattern around the entire North Pacific is preliminary and needs to be further confirmed by longer datasets and more elaborate analysis techniques. In fact, the space–time evolution is far from simple or obvious. Therefore, caution should be used when interpreting the results.

Acknowledgments. The authors would like to thank colleagues and staff from the NODC Ocean Climate Laboratory for their help in many aspects, particularly to John Antonov and Tim Boyer. Discussions with Professor Lewis Rothstein were very helpful. The authors wish to thank two anonymous reviewers for their numerous comments and suggestions that helped to improve the original manuscript. The authors are indebted to Profs. Qing-Cun Zeng and You-Lin Liang from the Institute of Atmospheric Physics, Chinese Academy of Sciences (Beijing, China) for their support of this work. This research was supported by the NOAA Climate and Global Change Program and the Chinese Ecosystem Research Network Program.

REFERENCES

Antonov, J. I., 1993: Linear trends of temperature at intermediate and deep layer of the North Atlantic and North Pacific Oceans: 1957–1981. *J. Climate,* **6,** 1928–1942.

Barnett, T. P., 1981: On the nature and causes of large-scale thermal variability in the central North Pacific Ocean. *J. Phys. Oceanogr.,* **11,** 887–904.

Bjerknes, J., 1964: Atlantic air–sea interaction. *Advances in Geophysics*, Vol. 10, Academic Press, 1–82.

——, 1969: Atmospheric teleconnections from the equatorial Pacific. *Mon. Wea. Rev.,* **97,** 163–172.

Boyer, T., and S. Levitus, 1994: Quality control of historical temperature, salinity, and oxygen data. NOAA Tech. Rep. NESDIS Tech. Rep. 81, 64 pp. [Available from NODC/NOAA, E/OC5, 1315 East West Highway, Silver Springs, MD 20910.]

Cayan, D. R., 1992: Latent and sensible heat flux anomalies over the northern oceans: Driving the sea surface temperature. *J. Phys. Oceanogr.,* **22,** 859–881.

Dickson, R., J. Meincke, S. Malmberg, and A. Lee, 1988: The ''Great Salinity Anomaly in the northern North Atlantic 1968–1982''. *Progress in Oceanography*, Vol. 20, Pergamon Press, 103–151.

Deser, C., M. A. Alexander, and M. S. Timlin, 1996: Upper-ocean thermal variations in the North Pacific during 1970–1991. *J. Climate,* **9,** 1840–1855.

Ebbesmeyer, C., D. R. Cayan, D. R. McLain, F. H. Nichols, D. H. Peterson, and K. T. Redmond, 1991: 1976 step in the Pacific climate: Forty environmental changes between 1968–75 and 1977–1984. *Proc. Seventh Annual Pacific Climate Workshop*, California Dept. of Water Resource, 115–126.

Graham, N. E., 1994: Decadal scale variability in the tropical and North Pacific during the 1970s and 1980s: Observations and model results. *Climate Dyn.,* **10,** 135–162.

Haney, R. L., 1980: A numerical case study of the development of large-scale thermal anomalies in the central North Pacific Ocean. *J. Phys. Oceanogr.,* **10,** 541–556.

Intergovernmental Oceanographic Commission, 1992: *Oceanic interdecadal climate variability.* IOC Technical Series, Vol. 40, UNESCO, 40 pp.

Jacobs, G. A., H. E. Hurlburt, J. C. Kindle, E. J. Metzger, J. L. Mitchell, W. J. Teague, and A. J. Wallcraft, 1994: Decade-scale trans-Pacific propagation and warming effects of an El Niño anomaly. *Nature,* **370,** 360–363.

Kawamura, R., 1994: A rotated EOF analysis of global sea surface temperature variability with interannual and interdecadal scale. *J. Phys. Oceanogr.,* **24,** 707–715.

Kushnir, Y., 1994: Interdecadal variations in North Atlantic sea surface temperature and associated atmospheric conditions. *J. Climate,* **7,** 141–157.

Latif, M., and T. P. Barnett, 1994: Causes of decadal climate variability over the North Pacific and North America. *Science,* **266,** 634–637.

——, and ——, 1996: Decadal climate variability over the North

Pacific and North America: Dynamics and predictability. *J. Climate,* **9,** 2407–2423.

Levitus, S., 1989: Interpentadal variability of temperature and salinity at intermediate depths of the North Atlantic Ocean, 1970–74 versus 1955–59. *J. Geophys. Res.,* **94,** 6091–6131.

——, and T. P. Boyer, 1994: *World Ocean Atlas.* Vol. 4, *Temperature.* NOAA Atlas NESDIS 4, U.S. Government Printing Office, Washington, DC, 117 pp.

——, J. Antonov, and T. P. Boyer, 1994a: Interannual variability of temperature at 125 m depth in the North Atlantic Ocean. *Science,* **266,** 96–99.

——, T. P. Boyer, and J. Antonov, 1994b: *World Ocean Atlas.* Vol. 5, *Interannual Variability of Upper Ocean Thermal Structure,* NOAA Atlas NESDIS 5, U.S. Government Printing Office, 176 pp.

——, R. D. Gelfeld, T. P. Boyer, and D. Johnson, 1994c: Results of the NODC and IOC archaeology and rescue projects: Rep. 1. Key to Oceanographic Records Documentation 19, 73 pp. [Available from NODC/NOAA, E/OC5, 1315 East–West Highway, Silver Springs, MD 20910.]

——, J. Antonov, Z.-X. Zhou, H. Dooley, K. Selemenov, and V. Tereshchenkov, 1995: Decadal-scale variability of the North Atlantic Ocean. *Natural Climate Variability on Decade-to-Century Time Scales,* D. G. Martinson, K. Bryan, M. Ghil, M. M. Hall, T. R. Karl, E. S. Sarachik, S. Sarooshian, and L. D. Talley, Eds., National Academy Press, 318–324.

Luksch, U., and H. von Storch, 1992: Modeling the low-frequency sea surface temperature variability in the North Pacific. *J. Climate,* **5,** 893–906.

Miller, A. J., D. R. Cayan, T. P. Barnett, N. E. Graham, and J. M. Oberhuber, 1994a: The 1976–77 climate shift of the Pacific Ocean. *Oceanography,* **7,** 21–26.

——, ——, ——, ——, and ——, 1994b: Interdecadal variability of the Pacific Ocean: Model response to observed heat flux and wind stress anomalies. *Climate Dyn.,* **9,** 287–302.

Namias, J., 1959: Recent seasonal interactions between North Pacific waters and the overlying atmospheric circulation. *J. Geophys. Res.,* **64,** 631–646.

Nitta, T., and S. Yamada, 1989: Recent warming of tropical sea surface temperature and its relationship to the Northern Hemisphere circulation. *J. Meteor. Soc. Japan,* **67,** 375–383.

Tanimoto, Y., N. Iwasaka, K. Hanawa, and Y. Toba, 1993: Characteristic variations of sea surface temperature with multiple time scales in the North Pacific. *J. Climate,* **6,** 1153–1160.

Trenberth, K. E., and J. W. Hurrel, 1994: Decadal atmosphere–ocean variations in the Pacific. *Climate Dyn.,* **9,** 303–319.

von Storch, J. S., 1994: Interdecadal variability in a global coupled model. *Tellus,* **46A,** 419–432.

Wang, B., 1995: Interdecadal changes in El Niño onset in the last four decades. *J. Climate,* **8,** 267–285.

Watanabe, T., and K. Mizuno, 1992: Decadal changes of the thermal structure in the North Pacific. *Int. WOCE Newslett.,* **15,** 10–12.

White, W. B., and T. P. Barnett, 1972: A servomechanism in the ocean/atmosphere system of the mid-latitude North Pacific. *J. Phys. Oceanogr.,* **2,** 372–381.

Yamagata, T., and Y. Masumoto, 1992: Interdecadal natural climate variability in the western Pacific and its implication in global warming. *J. Meteor. Soc. Japan,* **70,** 167–175.